

# Exploring Constraint: Simulating Self-Organization and Autogenesis in the Autogenic Automaton

Stefan Leijnen<sup>1</sup>, Tom Heskes<sup>2</sup> and Terrence W. Deacon<sup>3</sup>

<sup>1</sup> Amsterdam University of Applied Sciences, Amsterdam, Netherlands.

<sup>2</sup> Radboud University Nijmegen, Nijmegen, Netherlands.

<sup>3</sup> University of California, Berkeley, CA, USA.

s.leijnen@hva.nl

## Abstract

Many origin of life theories argue that molecular self-organization explains the spontaneous emergence of structural and dynamical constraints. However, the preservation of these constraints over time is not well-explained because of the self-undermining and self-limiting nature of these same processes. A process called autogenesis has been proposed in which a synergistic coupling between self-organized processes preserves the constraints thereby accumulated. This paper presents a computer simulation of this process (the Autogenic Automaton) and compares its behavior to the same self-organizing processes when uncoupled. We demonstrate that this coupling produces a second-order constraint that can both resist dissipation and become replicated in new substrates over time.

## Introduction

Life's ability to resist degradation and persist in hostile environments is both ubiquitous and astonishing. Generation of structure, preservation by repair, and trait persistence through reproduction are perpetually organized in a continuous struggle against the destabilizing mechanisms of the second law of thermodynamics. Despite their often pivotal role in explaining the emergence of life, self-organizing processes are limited in their capacity to maintain structure (Prigogine and Stengers, 1984; King, 1982). A recently proposed theory suggests that, beyond mere self-organization, a synergistic coupling between self-organizing processes is a minimal requirement for life (Deacon, 2012). Through this higher-order linkage, the processes that generate structure may persistently recreate a capacity for self-creation, leading to robustness and a potential capacity for long-term sustenance and natural selection. An example of such an *autogenic* process, a proto-life model system called the *autogen* is described to illustrate how two self-organizing processes – reciprocal catalysis and self-assembly – maintain each other's boundary conditions and thereby mutually increase their probability of persistence over time.

Currently, the autogen model is a theoretical proposition that remains to be validated experimentally. As a step toward validation, this paper describes a series of simulation

experiments that investigate the self-organizing and self-preserving properties of the autogen model. A simplified particle system simulation called the Autogenic Automaton models the synergistic linkage of self-organizing processes that leads to the emergence of autogens.

## Second-Order Self-Organization

The nonlinear amplification that is typical for self-organization tends to push the thermodynamic conditions for further propagation toward the unfavorable (Haken, 2006). This may occur up to a point where the system is no longer far-from-equilibrium and the local thermodynamic entropy increase comes to a halt. For example, in a reciprocally catalytic set reaction rates may increase exponentially as more and more catalysts are produced, up until the point when not enough reactants are available for further propagation and the self-organizing process ends (Plasson et al., 2011). Alternatively, self-organization may break down due to unfavorable changes in external conditions. Considering the universal presence of self-organization in living systems, how can it be possible that organization persists long enough for complex organisms to come about?

When the product of an autocatalytic reaction enables a second autocatalytic reaction, which produces a reactant that enables the first (or a third, etc., as long as the causal chain is eventually closed), a so-called *hypercycle* emerges (Eigen and Schuster, 1979). Hypercycles represent one possible way in which self-organizing processes, autocatalytic cycles in this case, may be linked together in a dynamical process hierarchy. However, with respect to preventing dissipation this kind of second-order self-organization does not provide a sufficient solution: every autocatalytic cycle that the hypercycle consists of represents a potential weakest link, which may cause the fragile hypercycle to break down entirely when the reactants or energy necessary for the cycle are no longer available. Conversely, autogenesis suggests another type of second-order self-organization where two or more self-organizing processes not only promote each other, but also act as a supportive environment if one of them breaks down in such a way that their self-

undermining tendencies are reciprocally counteracted.

### Autogenesis

The formation of crystals through self-assembly is a self-organizing process as the probability of particle detachment decreases with the number of adjacent particles that keep it in place. This asymmetric process causes particles to cluster together, creating a spatial difference in particle locations. This difference, maintained by the probabilities of attachment and detachment, may be viewed as a constraint on the spatial distribution of particles. More generally, this reduction of variety of macroscopic states can be understood as a constraint producing process (Deacon, 2006).

In a reciprocally catalytic system, each reaction initially leads to an increased probability for another reaction to take place as more and more catalysts are created. Exponential growth ensues until the reactants are depleted. Reciprocal catalysis leads to exponential increase of reactions that is limited solely by the number of available reactants.

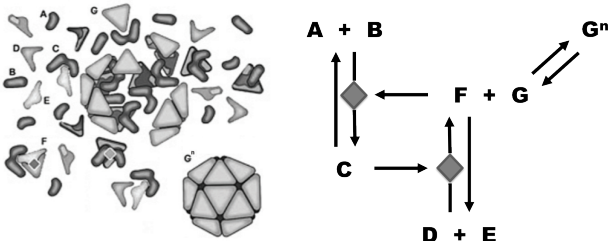


Figure 1: Illustration of autogen formation (left) and the reactions involved (right). Autogens constitute a dynamical linkage between self-assembly and reciprocal catalysis. In this model system, self-assembly is a self-organizing process where  $G$  particles attach to one another, forming  $G^n$  crystals of size  $n$ . These crystals may break up due to detachment.  $G$  particles are generated by a reciprocally catalytic set of six different particle types ( $A$  to  $F$ ). In turn, crystals may contain  $C$  and  $F$  particles, isolating these catalysts from potential reactants and thereby ensuring a potential for  $G$ -particle production over time.

A boundary or container would prevent the exhaustion of reactants by shielding them from the environment, thereby preserving a chemical potential for further dissipation (Maturana and Varela, 1980; Rosen, 1991). Such a container may itself be formed by a self-organizing process, e.g. crystal growth through self-assembly (Fellermann et al., 2007). Autogenesis (fig. 1) suggests that the form and function of a self-assembled container is dynamically linked to the catalytic process as it prevents the reactants from being depleted; similarly, it explains how the catalytic process dynamically shapes the form and function of the crystals as it affects the process of self-assembly.

Following the type of second-order self-organization described above as autogenesis, constraint preservation is enabled by a juxtaposition of constraint producing processes, such that they actively support each other's persistence. Whereas self-promoting self-organizing processes such as hypercycles tend toward self-undermining and ultimately a breakdown of the causal cycle, this reciprocally counteracting juxtaposition actively prevents self-undermining from taking place. As the autogen is able to do work on its own conditions for sustenance, it grows independent from the conditions of its environment and becomes more dependent on its internalized constraint. When the autogen is damaged, it likely begins to repair itself; under some conditions the probability of growth and sustainment may become higher than that of breakdown.

The relatively stability of these structural synergies allows for a simple type of natural selection to occur, as some will be better suited to prevailing conditions than others and therefore have a better chance of sustaining themselves. This eventually leads to a higher-level reduction of variety, as unsuccessful variety-reducing synergies are removed.

### The Autogenic Automaton

The processes that generate and preserve constraint and which are necessary for autogen formation are simulated in a program called the Autogenic Automaton. This simulation does not provide a physically accurate model, but is merely aimed at demonstrating the viability of the proposed constraint hierarchy (McMullin and Varela, 1997; Varela et al., 1974). A two-dimensional tile grid is used as a discrete model of a closed reaction-diffusion system (fig. 2). Six particle types are used for modeling reciprocal catalysis while a seventh type models the formation of crystals through self-assembly, following figure 1. Particle movement and the reaction rules that govern particle attachment, detachment, and the creation and removal of particles are all computed locally per tile. As such, the system resembles a cellular automaton (Bilotta and Pantano, 2005) where multiple particles may occupy one tile. Particle movement and diffusion caused by particle-to-particle collisions is approximated by random movement to a horizontally or vertically neighboring tile with a probability of 0.1 at every time step for each particle. With respect to movement, crystals are treated as single particles together with any particles they encapsulate.

The simulation is initialized by distributing predefined quantities of particle types randomly on the grid. Next, particle positions and reactions are computed per tile. Modeling only localized reactions ensures that only small subsets of the total number of particles interact at each time step, reducing the computational complexity of the simulation. Furthermore, only the aspects of self-organization that are necessary for demonstrating the viability of autogenesis are modeled. Physical properties such as kinetic energy, heat dissipation, and crystal geometry are not simulated. Due

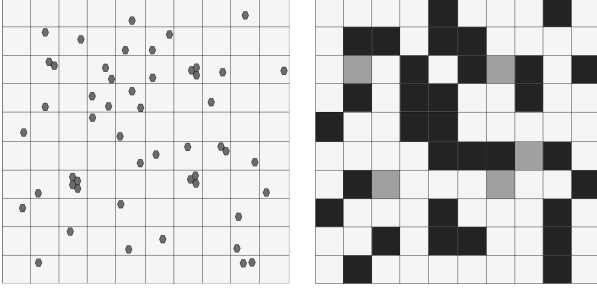


Figure 2: A closed continuous particle system (left) is modeled approximately in the Autogenic Automaton as a non-toroidal discrete grid of 10 x 10 tiles (right).

to this absence of heat and friction, the entropy potential necessary for far-from-equilibrium systems to become self-organizing is defined with respect to chemical equilibrium rather than thermodynamic equilibrium. The simulation is initialized with chemical non-equilibrium conditions, so before any crystallization has occurred or catalytic reactions have taken place.

### Quantifying Constraint

Through the course of a simulation run, the system moves through various macroscopic states caused by processes that generate, preserve and select constraint. Constraint can be expressed by the information entropy over the spatial probability distribution of particular event types in the tile grid (Kauffman, 1993; Harder and Polani, 2013; Polani, 2008). Notable characteristics of the particle system surface by observing the (in-)homogeneity of locations of events that correspond to these characteristics, such as the presence of a particle type or the occurrence of a reaction. The quantification of statistical entropy described below yields an indirect observation of the underlying processes.

Given a set of probabilities  $p_i$  for  $i = 1, \dots, n_{\text{tiles}}$  with  $0 \leq p_i \leq 1$  and  $\sum_i p_i = 1$ , the information entropy is defined as (Shannon, 1948; Cover and Thomas, 1991):

$$H = - \sum_{i=1}^{n_{\text{tiles}}} p_i \log_2 p_i .$$

When we consider an event  $X$ , we substitute

$$p_i = \frac{|X_i|}{|X|} ,$$

with  $|X_i|$  the number of events at tile  $i$  and  $|X| = \sum_i |X_i|$  the total number of events, to obtain

$$H(X) = - \sum_{i=1}^{n_{\text{tiles}}} \frac{|X_i|}{|X|} \log_2 \frac{|X_i|}{|X|} .$$

For ease of interpretation we often consider the so-called normalized information entropy (Jost, 2006)

$$\hat{H}(X) = - \frac{1}{\log_2 n_{\text{tiles}}} \sum_{i=1}^{n_{\text{tiles}}} \frac{|X_i|}{|X|} \log_2 \frac{|X_i|}{|X|} , \quad (1)$$

which normalizes the standard information entropy by its maximum value such that always  $0 \leq \hat{H}(X) \leq 1$ . For a completely homogeneous distribution of events over tiles we get  $\hat{H}(X) = 1$ , whereas  $\hat{H}(X) = 0$  when all events  $X$  are concentrated at a single tile.

Where it is necessary to measure the spatial difference between two event types,  $X$  and  $Y$ , the Kullback-Leibler divergence of their distributions over the grid is used (Kullback and Leibler, 1951):

$$D_{KL}(P||Q) = \sum_{i=1}^{n_{\text{tiles}}} p_i \log_2 \frac{p_i}{q_i} .$$

Substituting  $p_i$  and  $q_i$  with  $\frac{|X_i|}{|X|}$  and  $\frac{|Y_i|}{|Y|}$ , respectively, would yield infinite divergence for a distribution with a tile  $i$  such that  $|X_i| > 0$  and  $|Y_i| = 0$ . To resolve this problem, a smoothing function is used (Bigi, 2003), where

$$q_i = \begin{cases} \alpha \frac{|Y_i|}{|Y|} & \text{for } |Y_i| > 0 \\ \epsilon & \text{for } |Y_i| = 0 \end{cases} , \quad (2)$$

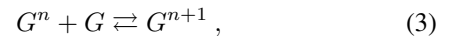
with  $\epsilon = 10^{-5}$  and normalization coefficient  $\alpha$  chosen such that the probabilities sum to 1.  $p_i$  is substituted similarly with  $\frac{|X_i|}{|X|}$ . For ease of exposition, we will omit this smoothing in subsequent formulas.

### Constraint Generation

The Autogenic Automaton is used here to simulate the generation of constraint in the formation of crystals through self-assembly and in the locally nonlinear of reactions taking place in a reciprocally catalytic set. In later sections, these two processes will be combined to simulate autogenesis.

### Self-Assembly

Self-assembly is modeled in a simplified way, by defining attachment and detachment reactions between  $G$  particles and crystals  $G^n$ :



with  $n \geq 1$  and  $G^1 \equiv G$ . At every time step, when a  $G$  particle is located within the same tile as either another  $G$  particle or crystal, the probability of attachment is given by reaction parameter  $\gamma^+$ :

$$P_g^+ = \gamma^+ \in [0, 1] .$$

Once formed,  $G$  particles have a probability  $P_g^-$  of detaching from the crystal again. Larger crystals are more tightly connected and less likely to break apart than smaller crystals due to a larger number of kinks holding the individual particles together (Burton and Cabrera, 1949). An increased size yields a lower probability of detachment and therefore increases the probability for further growth. This introduces asymmetry in the crystal growth process, reflected in our model system by a detachment probability function that is negatively exponential to the crystal size  $n$  with reaction parameter  $\gamma^-$ :

$$P_g^- = (1 + \exp[\gamma^-])^{-n},$$

with  $\gamma^- \in \mathbb{R}$ ,  $n \geq 2$ . Following equation (1), event  $X_i$  is defined with respect to self-assembly as the observation of a  $G$  particle at tile  $i$ , where  $G^n$  crystals are counted as  $n$  observations. Therefore, the generation of constraint during this process is examined using

$$\hat{H}(G, t) = -\frac{1}{\log_2 n_{\text{tiles}}} \sum_{i=1}^{n_{\text{tiles}}} \frac{|G_i(t)|}{|G(t)|} \log_2 \frac{|G_i(t)|}{|G(t)|},$$

for the normalized information entropy of  $G$  at time  $t$ .

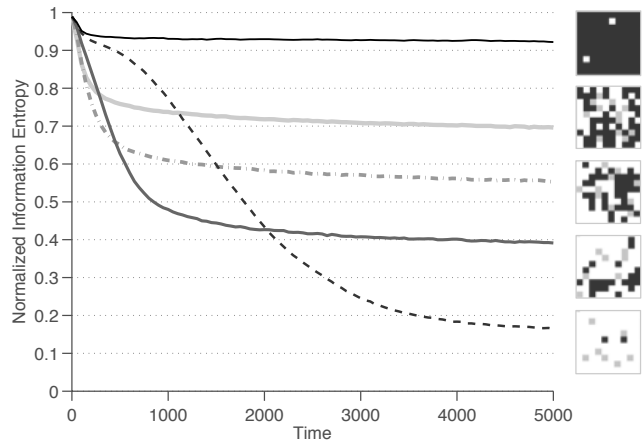


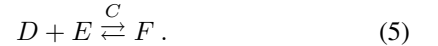
Figure 3: Decrease of normalized information entropy  $\hat{H}(G, t)$  during self-assembly of 1000  $G$  particles with  $\gamma^+ = 1$ , for several detachment probabilities: —  $\gamma^- = -5$ , - - -  $\gamma^- = -4$ , —  $\gamma^- = -3$ , - - -  $\gamma^- = -2$ , —  $\gamma^- = -1$ . The images on the right depict how  $\hat{H}(G, t)$  correlates with the distribution of  $G$  particles over the grid, ranging from an almost homogeneous distribution (top) to a few  $G^n$  crystals (bottom). Results are averaged over 100 trial runs.

Figure 3 shows the development of  $\hat{H}(G, t)$  over time, for different values of  $\gamma^-$ . With  $\gamma^- = -5$  the probability of detachment  $P_g^-$  is relatively high, leading many crystals to fall apart and the constraint on particle  $G$  locations being low.

With  $\gamma^- \in [-1, -2]$ ,  $P_g^-$  is relatively low: once formed, crystals only break apart sporadically, leaving hardly any  $G$  particles available for attachment and potential for further growth. At  $t = 5000$ , the  $G$  particle locations are maximally constrained for  $\gamma^- = -4$ .

### Reciprocal catalysis

Particle types  $A$  to  $F$  are used to model self-organization through reciprocal catalysis. Particles of type  $A$  and type  $B$  may react to form a  $C$  particle when both are located in the same tile; similarly for particles  $D$  and  $E$  forming  $F$ :



Particles  $F$  and  $C$  are catalysts for the left-to-right reactions of (eq. 4) and (eq. 5), respectively. Reaction probability  $P_r^+$  decreases exponentially with  $1/n$ ,  $n$  being the number of catalysts present at the same tile  $i$ , i.e.  $n = |F_i|$  for (4) and  $n = |C_i|$  for (5):

$$P_r^+ = (1 + \exp[\varrho^+])^{-(1+n)^{-2}},$$

with  $\varrho^+ \in \mathbb{R}$ . The right-to-left reactions (i.e.  $C$  splitting into  $A$  and  $B$  and  $F$  into  $D$  and  $E$ ) occurs with probability  $P_r^-$  for each  $C$  and  $F$  particle at every time step:

$$P_r^- = \varrho^- \in [0, 1].$$

Similar to self-assembly, reciprocal catalysis is a locally nonlinear process: one catalytic reaction increases the likelihood of another catalytic reaction occurring. However, the observable artifacts of reciprocal catalysis (i.e. the produced catalysts) may cease to exist once this amplification process no longer takes place, or they may diffuse to different locations. To quantify the generated constraint, we therefore use the probability distribution of reaction locations as observed events, rather than the locations of catalysts themselves. The constraint generated by reciprocal catalysis is quantified by a decrease in normalized information entropy. Following (eq. 1) event  $X_i$  is defined as the observation of catalytic reaction  $R$  at tile  $i$ :

$$\hat{H}(R, t) = -\frac{1}{\log_2 n_{\text{tiles}}} \sum_{i=1}^{n_{\text{tiles}}} \frac{|R_i(t)|}{|R(t)|} \log_2 \frac{|R_i(t)|}{|R(t)|}.$$

In order to investigate the effect of parameters  $\varrho^+$  and  $\varrho^-$  on the normalized information entropy,  $\hat{H}(R, t)$  is averaged over time:

$$\frac{1}{t_{\max}} \sum_{t=1}^{t_{\max}} \hat{H}(R, t).$$

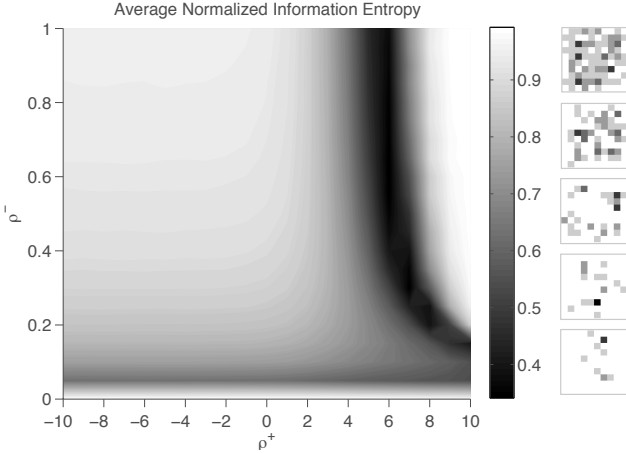


Figure 4: Normalized information entropy during reciprocal catalysis after initialization with 1000 particles distributed equally among types  $A$ ,  $B$ ,  $D$ , and  $E$ . For given  $\varrho^+$  and  $\varrho^-$ ,  $\hat{H}(R, t)$  is averaged over 5000 time steps and 10 trial runs. The right-side images depict the distribution of catalytic reactions over the grid.

Results for  $t_{\max} = 5000$  are shown in figure 4. It is found that distribution  $R$  is maximally constrained for  $\varrho^+ \approx 6$  and  $\varrho^- > 0.5$  (i.e. when catalysts break up regularly).

### Constraint Preservation

Under particular extrinsic conditions (i.e.  $\gamma^+$ ,  $\gamma^-$ ,  $\varrho^+$  and  $\varrho^-$ ) self-assembly and reciprocal catalysis generate constraint spontaneously. If these conditions are subject to unfavorable changes, the constraints produced will also be eliminated spontaneously. Here, we consider how a higher-order linkage between these processes may preserve constraint by preventing spontaneous dissipation in unfavorable conditions.

The autogenic process consists of a mutually constraining coupling.  $G$  particles generated by reciprocal catalysis are created in close proximity to one another due to the locality of catalytic amplifications, thereby increasing the likelihood of crystal growth; at the same time  $G^n$  crystals preserve a potential for reciprocal catalysis, by encapsulating catalysts and thereby preventing exhaustive catalysis.

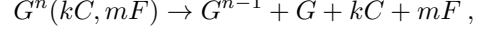
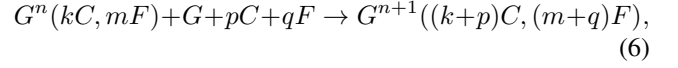
Modeling this synergetic linkage, the left-to-right reaction of (eq. 5) is changed as follows:



In order to balance out the production of  $G$  particles and keep the system (approximately) closed,  $G$  particles are removed from the simulation with probability  $P_g^- = (1 + \exp[\gamma^-])^{-1}$  for every  $G$  at each time step.

Crystals need to be capable of encapsulating catalysts upon formation, and release those again when breaking up.

This is reflected by changing reaction (eq. 3):



with  $k, m, p, q \geq 0$  and  $n \geq 2$ , and where a crystal of size  $n$  containing  $k C$  particles and  $m F$  particles is denoted as  $G^n(kC, mF)$ .

### Parameterization

The results in figure 3 show that a decrease in  $\hat{H}(G, t)$  may occur when  $\gamma^+$  is fixed at 1. Similarly, figure 4 shows that  $\varrho^- > 0.5$  allows for relatively low values of  $\hat{H}(R, t)$ . Here, we investigate the ranges of  $\gamma^-$  (horizontal axis) and  $\varrho^+$  (vertical axis) that allow for self-assembly and reciprocal catalysis to occur simultaneously.

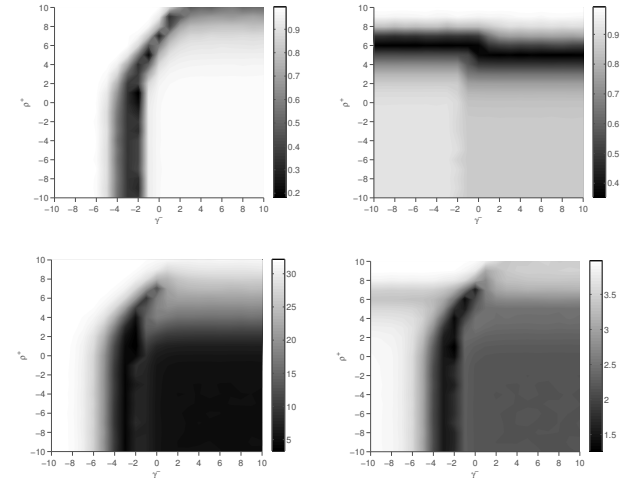


Figure 5: After initializing the simulation with 1000 particles uniformly distributed among types  $A$ ,  $B$ ,  $D$  and  $E$ , we run it for 5000 time steps with  $\gamma^+ = 1$ ,  $\varrho^- = 0.5$  and  $\gamma^-, \varrho^+ \in [-10, 10]$ . The four figures above show the average normalized information entropy of  $G$  particle locations (top left), the average normalized information entropy of catalytic reaction locations (top right), the average symmetrized Kullback-Leibler divergence with smoothing, where  $SD_{KL}(\gamma^-, \varrho^+) = \max(SD_{KL})$  if no occurrences are found (bottom left), and the sum of these three figures, where  $SD_{KL}$  has been normalized using scaling coefficient  $\beta$  (bottom right).

The redundancy between the distributions of  $G$  particle locations and catalytic reactions is considered to be an indication of the amount of interaction, i.e. it measures whether crystals tend to be located in proximity to catalytic reactions and vice versa. This redundancy is quantified using the

Kullback-Leibler divergence with smoothing (eq. 2), which is symmetrized to obtain a commutative measure:

$$SD_{KL}(G, R, t) = D_{KL}(G(t)||R(t)) + D_{KL}(R(t)||G(t)) \\ = \sum_{i=1}^{n_{\text{tiles}}} \left[ \frac{|G_i(t)|}{|G(t)|} - \frac{|R_i(t)|}{|R(t)|} \right] \log_2 \left[ \frac{|G_i(t)|}{|G(t)|} / \frac{|R_i(t)|}{|R(t)|} \right],$$

with smoothing (eq. 2) applied if necessary.

Autogenesis requires that self-assembly and reciprocal catalysis both take place in each other's proximity (fig. 5). The desired values for parameters  $\gamma^-$  and  $\varrho^+$  are therefore estimated by minimizing

$$\hat{H}(G, t) + \hat{H}(R, t) + \beta SD_{KL}(G, R, t),$$

where coefficient  $\beta$  scales  $SD_{KL}(G, R, t)$  to  $[0, 2]$

$$\beta = 2 \left( \max_{\gamma^-, \varrho^+ \in [-10, 10]} SD_{KL}(G, R, t) \right)^{-1}$$

such that the normalized information entropies and the divergence between the distributions contribute equally to the sum.

## Comparison

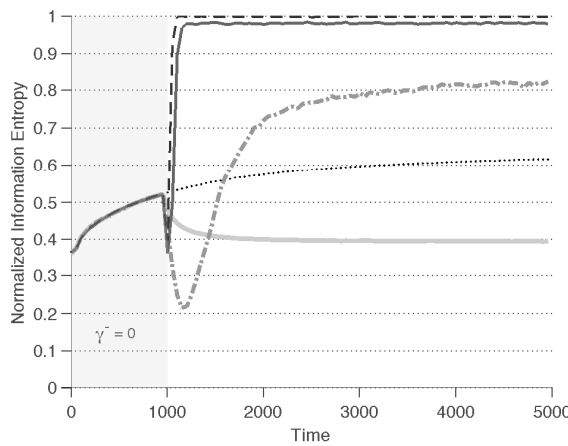


Figure 6: Normalized information entropy  $\hat{H}(G, t)$  during autogenesis, with  $\gamma^+ = 1$ ,  $\varrho^+ = 6$ ,  $\varrho^- = 0.5$ , and  $\gamma^- = 0$  for  $t \in [0, 1000]$ , and 1000 particles evenly distributed among types A, B, D and E initially. For  $t \in [1001, 5000]$ ,  $\cdots \gamma^- = -4$ ,  $\text{---} \gamma^- = -3$ ,  $\text{---} \gamma^- = -2$ ,  $\text{---} \gamma^- = -1$ ,  $\cdots \gamma^- = 0$ . Results are averaged over 1000 trials.

Figure 6 shows the normalized information entropy when, after an initial phase with conditions that enable self-assembly, the value of  $\gamma^-$  is changed. For  $\gamma^- \in [-5, -4]$  after  $t = 1000$ , the high probability of detachment is not conducive for the prolonged persistence of crystals, and they

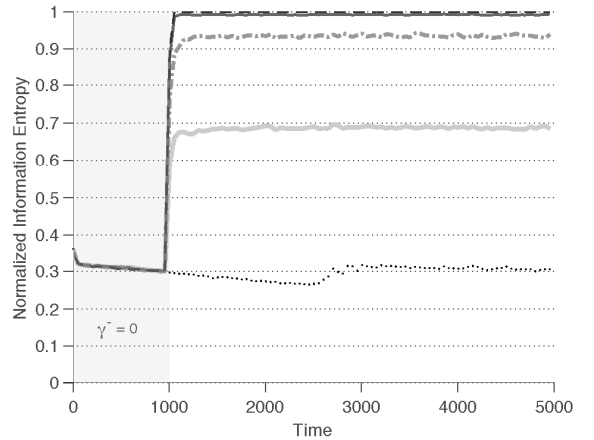


Figure 7: Normalized information entropy  $\hat{H}(G, t)$  during self-assembly (without reciprocal catalysis). Here, instead of being generated by a catalytic reaction,  $G$  particles are added to random grid locations at the same rate as in the previous simulation (see fig 6). Again,  $\gamma^+ = 1$ ,  $\varrho^+ = 6$ ,  $\varrho^- = 0.5$ , and  $\gamma^- = 0$  for the first 1000 time steps, while thereafter  $\cdots \gamma^- = -4$ ,  $\text{---} \gamma^- = -3$ ,  $\text{---} \gamma^- = -2$ ,  $\text{---} \gamma^- = -1$ ,  $\cdots \gamma^- = 0$ . Results are averaged over 1000 trials.

fall apart. For  $\gamma^-$  at 0,  $\hat{H}(G, t)$  continues to develop unperturbed. Changing  $\gamma^-$  to  $-1$  results in a lower normalized information entropy, as more  $G$  particles detach and subsequently attach to larger crystals (cf. fig. 3). With  $\gamma^-$  changed to  $-2$ ,  $\hat{H}(G, t)$  initially drops and eventually finds a new equilibrium at a value higher than with  $\gamma^- \in [-1, 0]$ .

Figure 7 shows a similar experiment where the particles necessary for reciprocal catalysis ( $A$  to  $F$ ) are omitted from the experiment. Here,  $G$  particles are added at random grid locations at the same rate as they were generated by reciprocal catalysis in the previous experiment. Spatial proximity is therefore no longer biased by reciprocal catalysis and the absence of catalysts excludes the possibility of encapsulation.

Comparing both figures, we find that for  $\gamma^- = -2$  constraint is preserved when a synergistic linkage between self-assembly and reciprocal catalysis is present while it largely falls apart in the case of mere self-assembly. Also for  $\gamma^- = -1$ , the value of  $\hat{H}(G, t)$  remains lower with this linkage than without it. These particular changes to  $\gamma^-$  show that an autogen may resist dissipation despite unfavorable extrinsic conditions; the intrinsic dynamical constraint between self-assembly and reciprocal catalysis allow it to persist.

## Constraint Selection

The preservation of dynamical constraint is a higher-order process: not only is the number of macroscopic states re-

duced as the spatial distribution of events becomes more constrained, but the distribution over specific constraint types (e.g. the specific form of crystals) is itself also reduced. To experimentally quantify this second-order reduction we initialize each newly formed crystal with a property  $c$ , a random integer between 1 and 5 that affects equation (6) by limiting the total number of catalysts that a crystal may contain. This property  $c$  reflects how the shape of a crystal may affect its containment capacity (fig. 8) without explicitly modeling the physical geometry of crystals.

The experiments of figures 6 and 7 are repeated while crystals are assigned random values for  $c$ . The average size of crystals is shown in figure 9.



Figure 8: Due to the way  $G$  particles attach to one another, crystals with different geometries may come about. This illustration shows several crystals  $G_c^n$  of equal size (i.e.  $n = 5$ ) but with different capacities ( $c$ ) for containing catalysts due their particular shape.

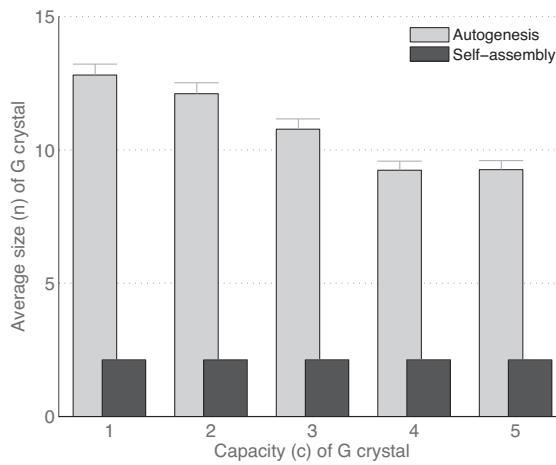


Figure 9: Fixing  $\gamma^-$  at  $-0.5$  and  $\gamma^+ = 1$ ,  $\varrho^+ = 6$ , and  $\varrho^- = 0.5$ , the grid is again initialized with 1000 particles of types  $A$ ,  $B$ ,  $D$  and  $E$ . For 1000 trial runs over 5000 time steps, the mean crystal size and standard error of the mean are reported for the five different containment capacities.

The difference in average crystal size between autogenesis and self-assembly can be inferred from the results of the previous experiments. However, the competition between crystals with different  $c$  leads to a second notable difference: the size of an autogen appears to be correlated with its containment capacity. In our simulation the geometry of a crystal does not affect its size directly, as the probabilities of crystal formation and detachment are independent of  $c$ .

Rather, the value of  $c$  affects the size of crystals indirectly, as the numbers of catalysts in a tile affects the production of new  $G$  particles, and thereby the crystal's capacity for reconstitution if those catalysts are released upon detachment. This work cycle creates a difference in size between crystal geometries, a difference which is maintained despite the absence of a direct causal link between crystal geometry and the underlying self-organizing processes.

This higher-order constraint is quantified using the normalized information entropy over the distribution of the containment capacities of crystals. With  $p_c$  the probability that a crystal has a containment capacity  $c$ ,  $|G_c^n|$  the number of crystals with capacity  $c$  and  $|G^n| = \sum_c |G_c^n|$  the total number of crystals,

$$p_c = \frac{|G_c^n|}{|G^n|},$$

$$\hat{H}(G_c^n, t) = -\frac{1}{\log_2 5} \sum_{c=1}^5 \frac{|G_c^n(t)|}{|G^n(t)|} \log_2 \frac{|G_c^n(t)|}{|G^n(t)|}.$$

Figure 10 shows the average  $\hat{H}(G_c^n, t)$  for the previous experiments. Selection of crystal geometries accounts for the difference in normalized information entropy over containment capacities during autogenesis.

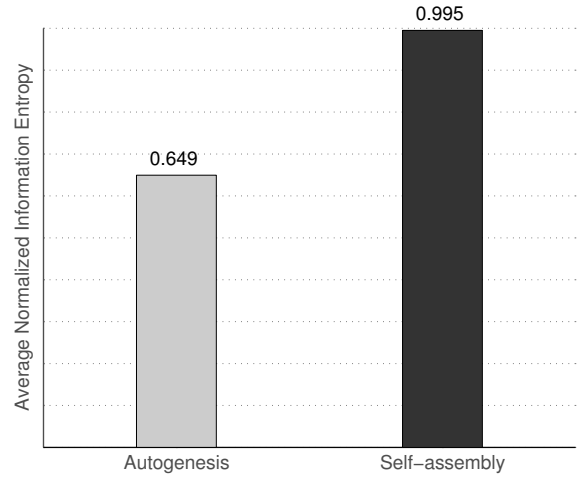


Figure 10: Higher-order constraint: the average normalized information entropy over the distribution of crystal capacities  $\hat{H}(G_c^n, t)$  is substantially lower for autogenesis (self-assembly + reciprocal catalysis) than for self-assembly alone. Results averaged over 1000 trial runs.

## Conclusions

The statistical distributions used to quantify self-organization and autogenesis in this paper ( $G$  particle

locations,  $R$  reaction locations, and  $G_c^n$  containment capacities) are all expressed in terms of information entropy. This type of quantification does not distinguish between the physico-chemical constraints produced by self-organization and the substrate independent, formal constraint made possible by autogenesis. Taking the physical processes that underlies the maintenance of far-from-equilibrium states into account requires further research (Beer, 2004). New tools capable of expressing this dynamical difference need to be developed (Deacon and Koutroufinis, 2014).

The experimental explorations described in this paper do not quantify all aspects of autogenesis, nor do they provide a complete overview of autogenic properties and phenomena. Rather, they serve to demonstrate the preservation capacity of synergetically coupled processes, and the higher-order reduction of macrostates constituted by formal type selection that may emerge from competition between autogens. These two autogenic capacities may help explain the possible emergence of proto-life. Understanding life's origins does not necessarily imply understanding life as we find it around us today (Cleland, 2013), but the emergent dynamics that created life may also take part in shaping mind and society (Thompson, 2010) as the accumulation of generated constraints that is allowed by preservation through a higher-order linkage is what ultimately makes selection possible.

## References

- Beer, R. D. (2004). Autopoiesis and cognition in the Game of Life. *Artificial Life*, 10(3):309–326.
- Bigi, B. (2003). Using Kullback-Leibler distance for text categorization. In *Proceedings of the 25th European Conference on IR Research*, ECIR'03, pages 305–319, Berlin, Heidelberg. Springer-Verlag.
- Bilotta, E. and Pantano, P. (2005). Emergent patterning phenomena in 2D cellular automata. *Artificial life*, 11(3):339–362.
- Burton, W. K. and Cabrera, N. (1949). Crystal growth and surface structure. Part I. *Discuss. Faraday Soc.*, 5:33–39.
- Cleland, C. E. (2013). Conceptual challenges for contemporary theories of the origin(s) of life. *Current Organic Chemistry*, 17:1704–1709.
- Cover, T. M. and Thomas, J. A. (1991). *Elements of Information Theory*. Wiley.
- Deacon, T. W. (2006). Reciprocal linkage between self-organizing processes is sufficient for self-reproduction and evolvability. *Biological Theory*, 1(2):136–149.
- Deacon, T. W. (2012). *Incomplete Nature: How Mind Emerged from Matter*. W.W. Norton and Company, New York, NY.
- Deacon, T. W. and Koutroufinis, S. A. (2014). Complexity and dynamical depth. *Information*, 5(3):404–423.
- Eigen, M. and Schuster, P. (1979). *The Hypercycle - A Principle of Natural Self-Organization*. Springer, Heidelberg.
- Fellermann, H., Rasmussen, S., Ziock, H.-J., and Solé, R. V. (2007). Life cycle of a minimal protocell—a dissipative particle dynamics study. *Artificial Life*, 13(4):319–345.
- Haken (2006). *Information and self-organization: a macroscopic approach to complex systems*. Springer.
- Harder, M. and Polani, D. (2013). Self-organizing particle systems. *Advances in Complex Systems*, 16.
- Jost, L. (2006). Entropy and diversity. *Oikos*, 113:363–375.
- Kauffman, S. A. (1993). *Origins of Order: self-organization and selection in evolution*. Oxford University Press, New York, NY.
- King, G. A. (1982). Recycling, reproduction, and life's origins. *Biosystems*, 15:89–97.
- Kullback, S. and Leibler, R. (1951). On information and sufficiency. *The Annals of Mathematical Statistics*, 22(1):79–86.
- Maturana, H. R. and Varela, F. J. (1980). *Autopoiesis and cognition*. Reidel, Boston, MA.
- McMullin, B. and Varela, F. J. (1997). Rediscovering computational autopoiesis. In Husbands, P. and Harvey, I., editors, *Fourth European Conference on Artificial Life*, pages 38–48. MIT Press, Cambridge, MA.
- Plasson, R., Brandenburg, A., Jullien, L., and Bersini, H. (2011). Autocatalysis: At the root of self-replication. *Artificial Life*, 17(3):219–236.
- Polani, D. (2008). Foundations and formalizations of self-organization. *Advances in Applied Self-Organizing Systems*, pages 19–37.
- Prigogine, I. and Stengers, I. (1984). *Order Out of Chaos*. Bantam Books, New York, NY.
- Rosen, R. (1991). *Life itself: A Comprehensive Inquiry into the Nature, Origin, and Fabrication of Life*. Columbia University Press, New York.
- Shannon, C. E. (1948). A mathematical theory of communication. *Bell Systems Technical Journal*, 27:379–423.
- Thompson, E. (2010). *Mind in Life*. Harvard University Press, Cambridge, MA.
- Varela, F. J., Maturana, H. R., and Uribe, R. (1974). Autopoiesis: The organization of living systems, its characterization and a model. *BioSystems*, 5:187–196.